



UNIVERSITÀ  
DEGLI STUDI  
FIRENZE

## FLORE

# Repository istituzionale dell'Università degli Studi di Firenze

### LES FOR THE EVALUATION OF ACOUSTIC DAMPING OF EFFUSION PLATES

Questa è la Versione finale referata (Post print/Accepted manuscript) della seguente pubblicazione:

*Original Citation:*

LES FOR THE EVALUATION OF ACOUSTIC DAMPING OF EFFUSION PLATES / Antonio Andreini; Cosimo Bianchini; Bruno Facchini; Antonio Peschiulli; Ignazio Vitale. - ELETTRONICO. - (2012), pp. 1-10. ( Proceedings of the Asme Turbo Expo Copenhagen 2012) [10.1115/GT2012-68792].

*Availability:*

The webpage <https://hdl.handle.net/2158/795065> of the repository was last updated on

*Publisher:*

ASME

*Published version:*

DOI: 10.1115/GT2012-68792

*Terms of use:*

Open Access

La pubblicazione è resa disponibile sotto le norme e i termini della licenza di deposito, secondo quanto stabilito dalla Policy per l'accesso aperto dell'Università degli Studi di Firenze (<https://www.sba.unifi.it/upload/policy-oa-2016-1.pdf>)

*Publisher copyright claim:*

La data sopra indicata si riferisce all'ultimo aggiornamento della scheda del Repository FloRe - The above-mentioned date refers to the last update of the record in the Institutional Repository FloRe

(Article begins on next page)

GT2012-68792

## LES FOR THE EVALUATION OF ACOUSTIC DAMPING OF EFFUSION PLATES

A. Andreini, C. Bianchini, B. Facchini

Department of Energy Engineering "Sergio Stecco"  
Via Santa Marta, 3 - 50139 Firenze, Italy  
cosimo.bianchini@htc.de.unifi.it

A. Peschiulli, I. Vitale

AVIO Group s.p.a., Torino  
Via I Maggio, 56 - 10040 Rivalta di Torino, Italy

### ABSTRACT

Effusion cooled liners, commonly used in gas turbine combustion chambers to reduce wall temperature, may also help reducing the propagation of pressure fluctuations due to thermoacoustic instabilities.

Large Eddy Simulations were conducted to accurately model the flow field and the acoustic response of effusion plates subject to a mean bias flow under external sinusoidal forcing. Even though existing lower order computational models showed good predicting capabilities, it is interesting to verify directly the influence of those parameters such as the staggered arrangement, the hole inclination, the presence of a grazing flow and the level of bias flow, which are not fully included in those models.

A first bi-periodic single hole configuration with normal acoustic forcing was selected to investigate the acousting behavior with varying inclination angle, bias and grazing flow. 90° and 30° perforations were simulated for bias flow Mach number in the range 0.05-0.1 and grazing flow between 0 and 0.08. Those conditions were chosen to expand the knowledge of acoustic properties towards actual liners working conditions. A second more computationally expensive set-up, including 4 inclined holes at 30°, focused on the damping of parallel to the plate waves.

Details of the computational methods implemented in the general purpose open-source unstructured CFD code OpenFOAM® exploited to conduct this analysis are reported together with an analysis of the results obtained from the acoustic computations both regarding the flow field generated and the absorption and energy dissipation coefficient.

### NOMENCLATURE

$a$	hole radius	[mm]
$A$	absorption coefficient	
$D$	hole diameter	[mm]
$f$	frequency	[Hz]
$h$	plate thickness	[mm]
$\mathcal{L}_i$	characteristic wave amplitude variation	
$j$	imaginary number	
$Ma$	Mach number	
$Ma_b$	Bias flow Mach number	
$Ma_{cf}$	Cross-flow Mach number	
$p$	static pressure	[Pa]
$P^+$	progressive pressure wave	[Pa]
$P^-$	regressive pressure wave	[Pa]
$R$	reflection coefficient	
$S_x$	axial spacing	[mm]
$S_y$	tangential spacing	[mm]
$S$	artificial pressure gradient	[kg/(m <sup>2</sup> s <sup>2</sup> )]
$t$	time	[s]
$T$	temperature	[K]
$u_1$	velocity normal to the boundary	[m/s]
$u_2, u_3$	velocity tangential to the boundary	[m/s]
$U$	velocity vector	[m/s]
$x$	stream wise direction/position	[m]
$y$	span wise direction/position	[m]
$z$	normal to plate direction/position	[m]
<b>Greeks</b>		
$\alpha$	energy dissipation coefficient	
$\beta$	relaxation coefficient	

$\lambda_i$	characteristic wave velocities	
$\theta$	hole inclination angle	[°]
$\phi$	phase	[rad]
$\mu$	dynamic viscosity	[kg/(ms)]
$\rho$	density	[kg/m <sup>3</sup> ]
$\sigma$	porosity,	[%]
	NSCBC reflection coefficient	
$\tau^{SGS}$	subgrid stress tensor	[%]

### Superscripts

'	fluctuating part
+	dimensionless in viscous units, downstream propagating wave
−	upstream propagating wave
∞	farfield values

## INTRODUCTION

There has been in recent years a growing interest among the aero-engine research community in the study of possible methods to reduce pressure fluctuations in the combustion chamber caused by thermo-acoustic instabilities. In particular due to weight constraints and to high working temperatures, attention was posed on simple passive devices, such as perforated plates, already employed in that zone of the engine for cooling purposes. It is in fact known that perforated plates with bias flow act as dampers with regards to acoustic waves [1].

Despite the fact that simple numerical models to characterize those screens have been proposed [2–4] and successfully applied [1,5,6] also to relatively complex set-up under a wide range of flow condition, detailed CFD simulations [7–9] and large experimental campaigns [10–13] are more and more performed to increase the knowledge of the mechanisms ruling the phenomenon and expand the database of available geometries and flow conditions.

Surprisingly the use of fully 3D computational technique did not push researchers to investigate more complex models including globally three dimensional flow and acoustic conditions. Most of the reported works dealt with the basic set-up in which an orthogonally perforated plate with relatively low bias flow is reflecting a normally incident acoustic wave in absence of any mean flow in the liner itself [5, 7, 8]. This situation is however not fully realistic on actual combustor liners since perforations are usually inclined, the combustor is subjected to a mean flow and the main acoustic waves are travelling parallel to the plate. This last effect was firstly studied by Heuwinkel et al. [14] in which a plane wave running along a long duct was damped by a 90° perforation on its surface composed by two rows of holes and fed with bias flow from a plenum. They performed both an experimental and a numerical campaign exploiting URANS computations. Their numerical work, focused in the range of  $0 < Ma_b < 0.1$ , was only partially successful in predicting acous-

tic measurements; at high  $Ma_b$  the error was around 30% because of an incomplete resolution of the vortices developing at the hole exit due to a too coarse grid resolution.

As already stated, another effect generally not considered is the inclination of the perforations. Combustor liners perforations, adopted primarily for cooling reasons, generally implement hole arrays aiming at full coverage film protection. In order to guarantee adequate cooling performance it is necessary to blow high quantities of coolant and to maintain the cold flow as much closer to the wall as possible. This can be only achieved by using highly slanted perforations below 20° [15, 16]. The influence of an inclined perforation and the consequent grazing flow was studied by Eldredge et al. [17] considering a 30° perforation with an enlarged, with respect to real engine dimension, hole diameter of 5 mm. They investigated the acoustic behaviour at 10 different forcing frequencies from 89.335 to 893.35 Hz imposed by means of a fluctuating bias flow inflow velocity. Despite the good agreement found with Howe model modified to account for plate thickness, the authors stated that more computations were needed to completely characterize the grazing-bias flow acoustic interaction especially due to arising shear instabilities inside the aperture.

The aim of this paper is to consider all the above mentioned effects into the same investigation to completely characterize the perforation already investigated with a basic set-up in [6]. In practice the analysis includes the effects of slanted perforation (orthogonal and 30° holes), of a mean cross-flow and a non normal acoustic forcing as well as a two level analysis on the influence of the  $Ma_b$ .

The complete test matrix was computed in a single hole bi-periodic domain with normal acoustic forcing only but, in order to consider also parallel running waves, a multi-hole (4 rows perforation) case was simulated too.

Details of the proposed numerical techniques are given in the first part of the paper to provide an overview and a reference for the computational methodology. A systematic validation of the acoustic simulation procedure against both available experiments and lower order numerical tools was already carried out in [6] on simpler reference tests thus the focus of this work will be on the newly introduced technique only. Comparison with results obtained with lumped acoustic procedure (Howe model [18]) is included in the discussion.

## GEOMETRY AND FLOW CONDITIONS

As already mentioned, this work is focused on the estimation of the absorption properties of multiperforated plates with cylindrical holes only. To further reduce the number of parameters investigated, the diameter and the pitches are maintained constant, with values representative of real liner perforations as reported in Tab.1, guaranteeing a porosity  $\sigma = 1.17\%$ .

$S_x/D$	9.125
$S_y/D$	7.375
$h/D$	3.125

Table 1. Constant perforation properties

The investigated test matrix consider variable hole inclination and flow conditions, i.e. bias and grazing flow. Classical configuration for acoustic analysis dealing with  $90^\circ$  perforations is compared with an inclined hole at  $30^\circ$  which is more relevant for cooling purposes. Also the range of investigated flow conditions have been chosen to represent actual cooling systems flow regimes at least in terms of velocity field. Each parameter is varied on two level (L for low and H for high) as reported in Tab.2. In order to simplify the notation, each condition is identified by a code representing the inclination angle, the bias and the cross-flow condition, e.g. 30LH means  $30^\circ$  at low bias and high grazing flow, an additional I identify the cases with in-line hole arrangement.

	Low (L)	High (H)
$\theta$	$30^\circ$	$90^\circ$
$M_b$	0.05	0.1
$M_{cf}$	0	0.08

Table 2. Test matrix

Reference pressure ( $p_{REF} = 100000Pa$ ) and temperature ( $T_{REF} = 293.15K$ ) are maintained close to ambient conditions and no heat exchange is considered on the domain boundaries.

Concerning the adopted acoustic forcing, the amplitude is maintained in the linear regime to avoid undesired effects such as flow reversal, with maximum pressure level of 125 dB while the frequency range is limited between 550Hz and 1300 Hz. Even though the range of frequencies of interest is broader and involves also lower frequency contributions, the computational cost limited this enquiry as better explained in the following section.

## NUMERICAL METHODS

### LES solver

In order to resolve the turbulent acoustic fields, the open-source finite-volume toolbox OpenFOAM<sup>®</sup> [19] was used. In particular a pressure based solver implementing time resolved PISO loop for compressible flow was used [20]. The time integration steps were chosen for each calculation to maintain a maximum Courant number in the domain around 0.5 to improve solver stability and allow the use of second order centered scheme for the convective term together with a backward implicit Euler scheme for time integration.

Sub-grid stresses were modelled following the Smagorinsky approach. Even though near wall turbulence is supposed not to deeply influence the acoustic behaviour of the effusion plates, the sub-grid viscosity is corrected by means of VanDriest near wall damping [21]. In order to overcome typical near wall deficiencies of Smagorinsky model, the Wall Adaptive Local Eddy-viscosity model by Nicoud [22] was also implemented. Anyhow no sensible differences among the two SGS models were recorded in the validation and reference test case thus in the following results are presented with no reference to the model in use.

The computational grids were generated with ICEMCFD<sup>®</sup> software by means of a multi-block structured approach. Near wall grid requirements for wall resolved LES were satisfied clustering the grid close to the wall in all three directions ( $z^+ < 1$ ;  $x^+ < 100$ ;  $y^+ < 20$ ) [23]. A posteriori analysis were conducted in order to verify the far field grid requirements. Two criteria were employed to establish sufficient grid resolution in the interior of the domain: the modelled turbulent kinetic energy was checked to be less than 20% of total turbulent kinetic energy and the filter was verified to assume values only one order of magnitude higher than the Kolmogorov length scale, estimated using subgrid dissipation, everywhere in the domain. Global size of the meshes results to be  $670 \cdot 10^3$  cells for the  $90^\circ$  hole,  $840 \cdot 10^3$  for the single hole at  $30^\circ$  and  $4.3 \cdot 10^6$  for the multi-hole configuration.

However for a transient calculation mesh size is only partially responsible for the total computational cost and the number of iteration required plays a major role in the necessary CPU time. As it will be better described in the following sections, for an acoustic forcing at 1000 Hz the entire simulation time is 30 ms that in conjunction with a time step in between  $2.5 \cdot 10^{-7}$  for the multi-hole case and  $1 \cdot 10^{-6}$  for the  $90^\circ$  case results in a total amount of 120000 and 30000 iterations respectively. Calculations for the single hole cases were run on a 8 cores Intel Xeon X5472 at 3.00 GHz for more than 400 hours while the multi-hole model acoustic simulation took almost 800 hours on a 12 cores X3430 at 2.40 GHz.

## Characteristic Boundary Conditions

In order to simultaneously guarantee small levels of reflectivity on the boundaries and the desired mean conditions, the Navier Stokes Boundary Conditions proposed by Poinsot et al. [24] with Linear Relaxation Method [25] were adopted.

**NSCBC** NSCBC is a method based on the “characteristic lines” which inherits most concepts from Euler Characteristic boundary conditions (ECBC) methods by Thompson [26, 27] with an additional adaptation for the diffusive terms due to viscous and conductivity effects [28]. The concept behind ECBC and NSCBC is to impose boundary conditions in terms of characteristic waves amplitude variations  $\mathcal{L}_i$ . Those related to entering waves are calculated with information provided externally to maintain the desired mean flow while those related to the leaving waves are extrapolated from the interior of the domain. Outgoing wave amplitude variations can be specified by making the assumption that the flow in the boundary region is one dimensional and inviscid. If this is the case the relations of LODI (Local One Dimensional Inviscid problem) strictly applies. They should not be considered physical conditions but viewed as compatibility relations between the choices made for physical boundary conditions and the amplitudes of waves crossing the boundary [24].

Equations employed to compute outgoing amplitude variations are reported in Eq.1, where  $\lambda_i = (u_1 - c; u_1; u_1; u_1 + c)$  are the respective characteristic wave velocities.

$$\begin{aligned}\mathcal{L}_1 &= \lambda_1 \left( \frac{\partial p}{\partial x_1} - \rho c \frac{\partial u_1}{\partial x_1} \right) \\ \mathcal{L}_2 &= \lambda_2 \left( c^2 \frac{\partial p}{\partial x_1} - \frac{\partial p}{\partial x_1} \right) \\ \mathcal{L}_3 &= \lambda_3 \frac{\partial u_2}{\partial x_1} \\ \mathcal{L}_4 &= \lambda_4 \frac{\partial u_3}{\partial x_1} \\ \mathcal{L}_5 &= \lambda_5 \left( \frac{\partial p}{\partial x_1} + \rho c \frac{\partial u_1}{\partial x_1} \right)\end{aligned}\quad (1)$$

**LRM** For the incoming waves instead, it is necessary to specify the value of their amplitude variations in such a way to maintain the desired mean flow conditions without decrementing the non-reflective behaviour of the boundary itself. A technique to achieve this property is to relax the wave amplitude variation with respect to a specified reference value:

$$\begin{aligned}\mathcal{L}_1 &= \sigma_p (p - p^\infty) \\ \mathcal{L}_2 &= \sigma_T (T - T^\infty) \\ \mathcal{L}_3 &= \sigma_{u_2} (u_2 - u_2^\infty) \\ \mathcal{L}_4 &= \sigma_{u_3} (u_3 - u_3^\infty) \\ \mathcal{L}_5 &= \sigma_{u_1} (u_1 - u_1^\infty)\end{aligned}\quad (2)$$

This kind of procedure is commonly known as the Linear Relaxation Method (LRM) [25]. Appropriate values of the re-

laxation coefficients  $\sigma$  provide a partially reflecting behaviour for the boundary. If the relaxed variable drifts from its target value its corresponding wave amplitude variation acts as a linear spring force to push it back toward its target value. Thus the  $\sigma_i$  parameters should be chosen to match the correct inlet impedance.

**Acoustic forcing** A sinusoidal far-field pressure was applied in the LRM method to generate the desired acoustic forcing. Standard procedure would require to investigate one frequency at the time imposing a monotonal pressure signal at the outlet. However since not only a single frequency is of interest, the range of investigation is from 550 to 1300 Hz, and the computational cost of these simulations is quite relevant, a multi harmonic pressure wave, see Eq.3, was employed in order to save computational time.

$$p^\infty = p_{REF} + \sum_{i=1}^N p_{0,i} \cos(2\pi f_i t + \phi_i) \quad (3)$$

Additional post-processing procedures were necessary to decompose the sample pressure onto a composition of sinusoidal signals at the desired frequencies as reported in the following section.

Even though combustion instabilities provide a broadband low-frequency forcing, it is important to underline that high amplitude oscillations actually develop only at a given number of specific frequencies. Moreover experiments and other computational predictions generally perform such analysis investigating one frequency at the time [5], it is hence fundamental, to compare the responses of pure and multi-tonal signals in order to evaluate the effects of spurious forcing.

An analysis to assess the effect of multifrequency forcing compared to standard pure tone excitation was conducted on the reference test 90HLI. 3 single frequencies computations at (700, 1000 and 1300 Hz) are compared respectively with a dual frequency (1000 and 1300 Hz) and a narrow banded 4 tones signal (550, 700, 850 and 1150 Hz). Differences in the computed absorption coefficients are respectively around 1, 5 and 10% as reported in Fig.5. Since this kind of uncertainty is comparable to the one related to the number of time probes included in the post-processing procedure, in the following excitation is provided by means of a multi-composed pressure signal.

## Howe model

The proposed LES methodology is compared to a simplified approach which solve only for the acoustic field inside the liner and model the acoustic impedance of perforated plates with bias flow as an equivalent wall compliance, already presented in [6] and here briefly summarized.

Following the mathematical formulation of Dowling and Eldredge [4] and exploiting Howe [18] model with extension by Dowling and Hughes [29] to consider a regular pattern of holes, it is possible to relate the overall wall compliance  $\eta$  to the Rayleigh's conductivity  $K$  [30].

In such a way a special boundary condition was implemented within the acoustic module of the commercial solver COMSOL® to treat those perforated screens. Since only the acoustic field is solved for, this approach is insensitive to the presence of cross-flow thus these results will be reported for the no grazing flow configuration only.

## NORMAL WAVE

As already hinted, this set-up considers a single hole only assuming fully developed conditions and repeatability of the acoustic behaviour. A bi-periodic domain was implemented to include the effect of neighbouring holes as shown in Fig.1 in which lateral boundaries are coupled each other with periodic conditions. In case of desired mean cross-flow, it is generated across the two patches with normal vector oriented in the X direction, called in the following X+ and X-.

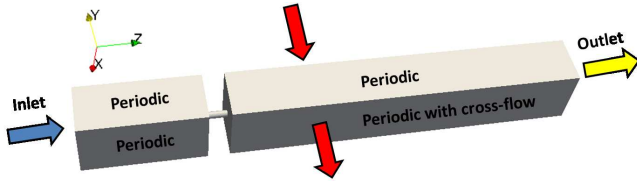
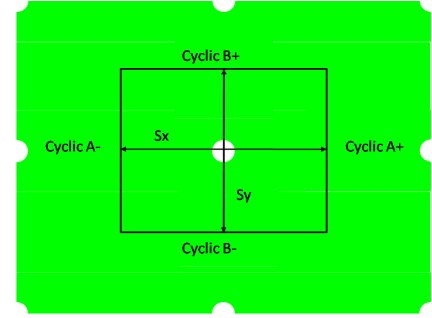


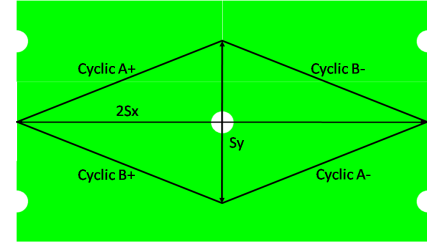
Figure 1. Normal wave case computational domain overview.

This domain definition enables to represent an infinite pattern of holes in both the stream and tangential direction and was already implemented for similar purposes in [5, 31]. Surfaces  $Y+$  and  $Y-$ , with normal vector orthogonal to the eventual main flow, reproduce a simple in-line arrangement as better reported in Fig.2(a). In order to consider typical staggered hole pattern, a different configuration needs to be employed, as reported in Figs.2(b) and 2(c). Even though arrangement in Fig.2(b) has already been successfully employed by other authors [17, 32, 33], with the aim of preserving high mesh quality also in case of high stream to tangential pitch ratio, the rectangular arrangement was chosen for this work.

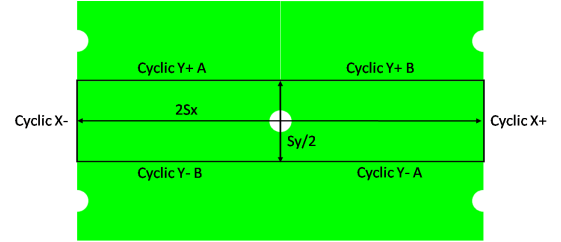
A fluctuating pressure at the outlet boundary, which generates a wave travelling perpendicular to the wall, is exploited to impose the acoustic forcing. The outlet is placed at a distance  $z = 110a$  from the perforated plate for each of the analysed cases, in order to be sufficiently far from the wall. The inlet patch is instead placed closer to the wall and the bias flow is generated by



(a) In-line domain



(b) Staggered Rhomboidal domain



(c) Staggered Rectangular domain

Figure 2. Domain definitions

a totally reflecting velocity inlet. Such a scheme is equivalent to that exploited by Mendez and Eldredge [5] and Andreini et al. [6].

## Multimicrophone method

To characterize the acoustic behaviour of the perforated plate in case of a normal acoustic excitation, it is necessary to reduce the 3D unsteady pressure field into an upstream  $p_1^+$  and a downstream  $p_1^-$  running wave as described in Fig.3.

The reflection coefficient can then be defined as the ratio between the reflected and the incident acoustic pressure waves to the obstacle, see Eq.4, and the absorption coefficient simply calculated from the reflection coefficient since the perpendicular

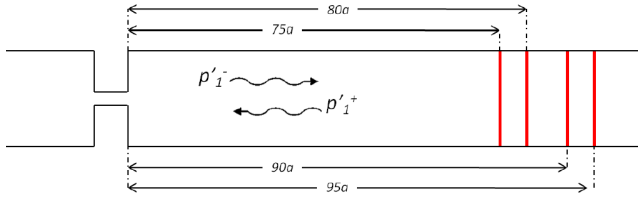


Figure 3. Sampling plane positions to apply the multi microphone technique.

wave excitation permits to reduce its expression to Eq.5.

$$R = \frac{p'_{1-}}{p'_{1+}} \quad (4)$$

$$A = 1 - R^2 \quad (5)$$

In order to evaluate  $A$  and  $R$ , hence to separate pressure contributions given by the concordant  $p'_{1-}$  and discordant  $p'_{1+}$  waves to the bias flow, the multi-microphone method [34] is applied to the pressure field of the acoustically excited solution.

Such technique aims to evaluate  $p'_{1-}$  and  $p'_{1+}$ , by means of a pressure sampling at various distances from the acoustic obstacle, corresponding to the perforated plate. By the imposition of compatibility conditions at the plate itself, the resulting equation for the pressure at position  $z_i$  as composition of the upstream and downstream running wave is reported in Eq.6. A least square approximation procedure is employed to calculate the values of  $p'_{1-}$  and  $p'_{1+}$  better reproducing the  $p(z_i, t)$  monitored at specified locations.

$$p(z_i, t) = \sum_k \left( P^+(f_k) \cdot e^{-j2\pi f_k / c z_i} + P^-(f_k) \cdot e^{j2\pi f_k / c z_i} \right) \cdot e^{-j2\pi f_k t} \quad (6)$$

In order to purge sampled data from initial transient behaviour and possible effects of non perfect averaging, 30 oscillating periods relatively to the lowest forcing frequency of the exciting signal are simulated, and only the latest 20 are considered during the post-processing phase. In fact, as stated in [1] and [35], this permits to reach well-developed statistically steady conditions to calculate the aeroacoustic parameters.

The pressure signal is sampled at four different sampling planes, where an area-average of fluctuating pressure is evaluated. Planes are chosen at the same distance from the solid wall for each analysed configuration, at distances  $z/a = 75, 80, 90, 95$  as reported in Fig.3. These are sufficiently far from the hole outlet to consider the hypothesis of plane pressure wave with a sufficient approximation.

### 90° in-line and staggered array

Before starting the acoustic simulation a fully-developed free jet simulation was run for each configuration investigated. In order to verify and validate the implemented periodic bound-

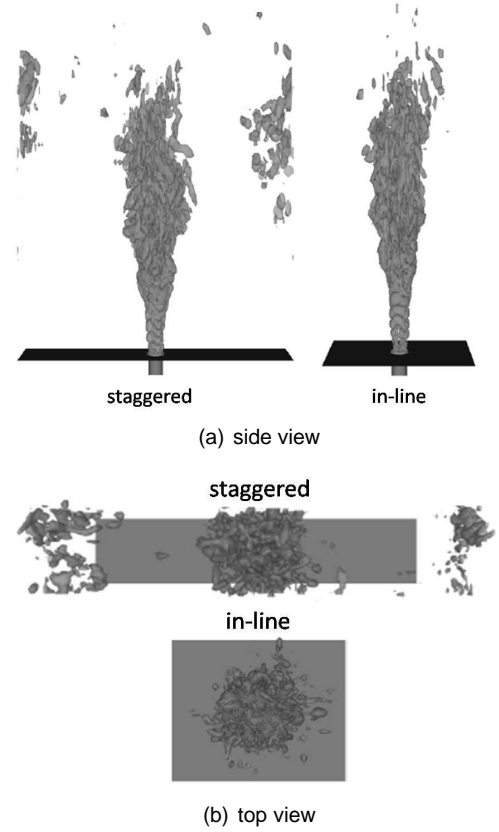


Figure 4. Isosurfaces of instantaneous velocity gradient second invariant.

ary treatment, isosurfaces of  $Q$  were extracted for the 90HH case (free jet configuration) in both the in-line and staggered calculations to highlight coherent turbulent structures. As it is possible to note in Fig.4 the effect of the periodic boundary is low and the two jets develop almost in the same manner showing equivalent jet length.

The acoustic simulations showed, see Fig.5, that the absorption coefficient is substantially equivalent for the two configurations even though the staggered array of holes results to be more influenced by the forcing frequency.

At low frequencies both a peak at 850 Hz and a local minimum at 700 Hz are evidenced. To purge possible effects of interactions between the forcing modes, additional pure tone simulations were conducted confirming the reported for the multifre-

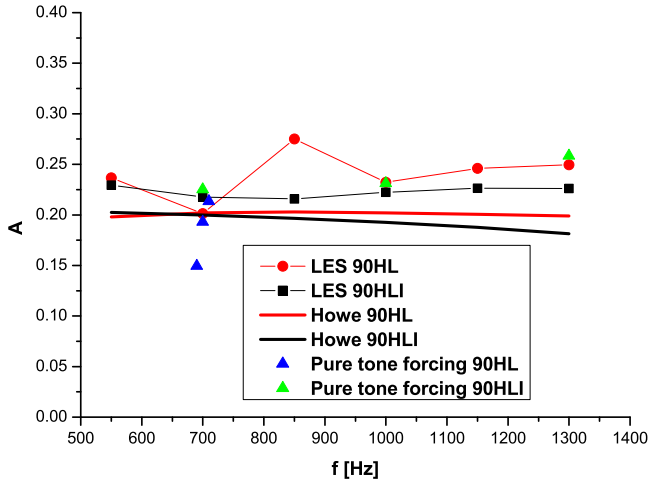


Figure 5. Staggered and in-line arrangement comparison ( $90^\circ$ ,  $Ma_b = 0.1$  and  $Ma_{cf} = 0$ ).

quency forcing (10% variation which is the expected uncertainty for this type of computations). A further analysis was carried out for  $f=690$  and  $710$  Hz to verify if the lower absorption was connected to some specific mode excitation related to the boundary conditions set-up. The absorptions obtained also for these two computations allow to conclude that the lower absorption is not limited to this specific frequency but is extended also for neighbouring frequencies, in particular minimal absorption is reported for  $690$  Hz. The causes for such discontinuous behavior were not totally identified yet.

Rayleigh conductivity model shows equivalent values of absorption, roughly 10% lower, with a much lower influence of the hole arrangement, this is consistent with the fact that in such a scheme the acoustic field is almost 1D and so independent on the lateral conditions imposed.

#### 90° effect of $Ma_b$

It is known that the level of bias flow is deeply influencing the absorption properties of the perforation: increasing the bias flow, the plate tends to behave like a rigid plate reflecting more and more the incident pressure wave [6, 11].

In Fig.6, the absorption coefficient for  $Ma_b = 0.1$  and  $Ma_b = 0.05$  is reported. The 90LL configuration shows almost constant absorption for  $f \geq 850$  Hz with a decrease for lower frequencies. The increase of absorption moving from high to low  $Ma_b$  is strong, ranging between 30% and 75%.

As already reported the quantitative agreement between LES and Howe model is quite good for the high bias case, for the low bias case instead LES predict a more pronounced increment at the higher frequencies while the acoustic solver predicts a decreasing absorption up to  $1000$  Hz.

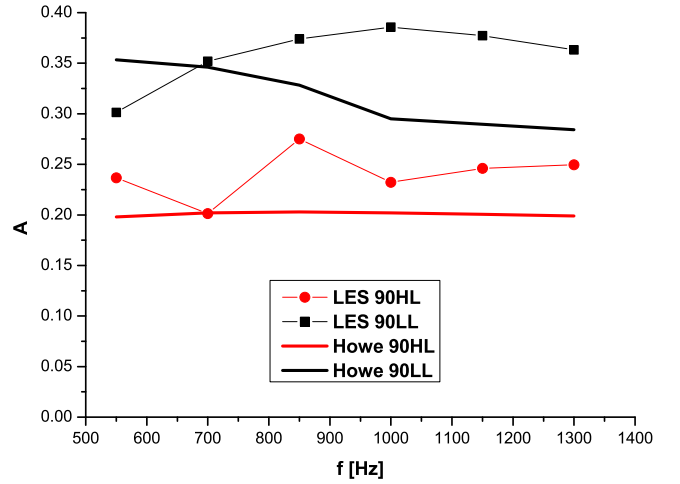


Figure 6. High and low bias flow absorption ( $90^\circ$ ,  $Ma_{cf} = 0$ ).

#### Modelling of crossflow

The described set-up is not directly employable to consider the effect of crossflow since periodic boundaries  $X^-$  and  $X^+$  cannot guarantee the adequate pressure difference to sustain the main flow. The grazing flow needs to be generated by other terms artificially introduced in the Navier-Stokes equations.

The idea is to opportunely modify the momentum equation, introducing an artificial source term driving the grazing flow, despite the fact that a natural mean pressure gradient in  $X$  direction is absent. The momentum equation was thus modified in this case as:

$$\rho \frac{\partial \bar{u}_i}{\partial t} + \rho \frac{\partial (\bar{u}_j \bar{u}_i)}{\partial x_j} + \frac{\partial \bar{p}}{\partial x_i} - \frac{\partial}{\partial x_j} \left( \mu \frac{\partial \bar{u}_i}{\partial x_i} - \tau_{ij}^{SGS} \right) = S_j \quad (7)$$

where  $S$  represents an artificial pressure gradient. Such term is a vector, only acting on the part of grid where the grazing flow is present. This could theoretically assume every distribution of values inside the domain, but to avoid further complications, it is simply chosen as constant in modulus and direction.

Because of the objective difficulty to identify the correct value of such term to generate the desired grazing flow, its value is automatically updated at each iteration as follows:

$$\begin{aligned} S^{n+1} &= S^n + \Delta S^n \\ \Delta S^n &= \beta (u_{cf}^n - u_{MEAN}^n) \end{aligned} \quad (8)$$

vector  $u_{cf}^n$  corresponds to the desired grazing flow velocity, whilst  $u_{MEAN}^n$  represents the mean volume averaged velocity at iteration  $n$ , computed in the zone where a non-null source term is required.  $S$  is automatically updated until the mean velocity field inside the domain equals the mean velocity value ( $u_{cf}$ ) imposed. According to Mendez and Nicoud [35] the relaxation coefficient  $\beta$  was chosen equal to  $\rho_{MEAN}/(10dt)$ , where  $dt$  is the simulation time step.

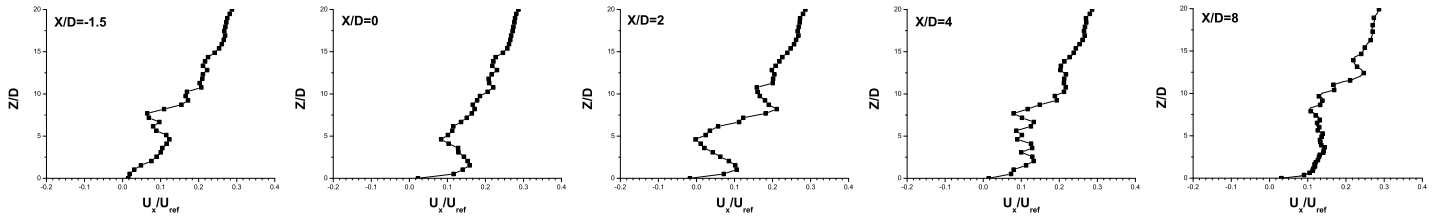


Figure 7. Mean streamwise velocity profiles for 90° case ( $Ma_b = 0.1$ ).

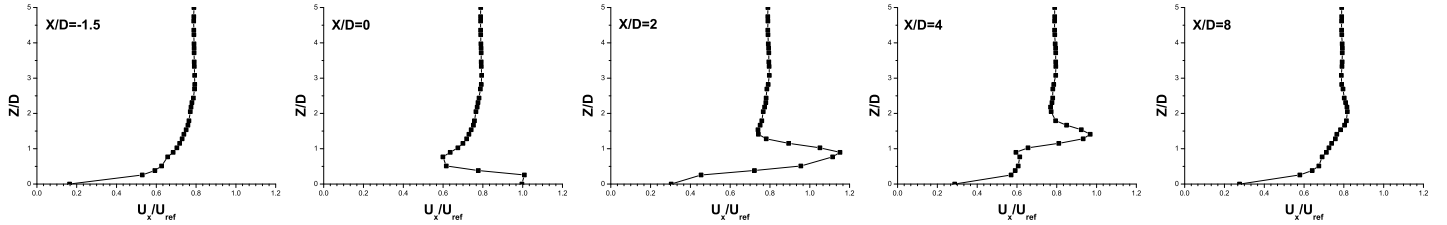


Figure 8. Mean streamwise velocity profiles for 30° case ( $Ma_b = 0.1$ ).

### 90° and 30° with cross flow

First thing to verify is the capability of the adopted source term to generate a realistic crossflow in the domain. Both the 90° and the 30° geometries were investigated for a  $Ma_{cf} = 0.08$ . The situation between the tests is substantially different since at 90°, there is no momentum injection in the crossflow direction, while at 30° the bias flow is promoting the generation of a mean grazing flow.

Figs.7 and 8 report the mean velocity profiles at various  $X$  positions along the centerline made dimensionless with respect to the reference velocity, i.e. bulk velocity in the hole. It is possible to note how these profiles are influenced by the jet only up to certain distance from the wall. For the 90° case a wake is noted up to  $Z/D=10$  while for the 30° a peak in streamwise velocity, due to  $VR \geq 1$ , is found up to  $Z/D=3$ . Moreover the axial spacing is sufficient to absorb the perturbations on the mean flow generated by the jet as the incoming profile is almost unperturbed at  $X/D=-$

1.5 at least for the inclined jet. The 90° case is not showing a flat cross-flow profile but is instead almost linearly increasing. This is due to the uniform distribution of the source term, necessary to generate the mean flow, that is much higher than at 30° since no stream momentum is injected from the hole. The two velocity profiles, quite different in the proximity of the plate, assume equivalent values of cross-flow in the far field region where the desired condition of  $Ma_{cf} = 0.08$  is achieved.

Concerning the effects on acoustic properties, the cross-flow is shown to weakly influence the absorption properties as reported in Fig.9. This comparison could only be performed for the 90° geometry since in streamwise periodic set-up it is not possible to maintain a null crossflow for an inclined perforation due to the slanted injection of fluid coming out from the hole.

The 30° geometry is so compared to the 90° case at  $Ma_{cf} = 0.08$ , see Fig.10, showing that the inclined perforation results in lower absorption capabilities, except at 700 Hz where the absorp-

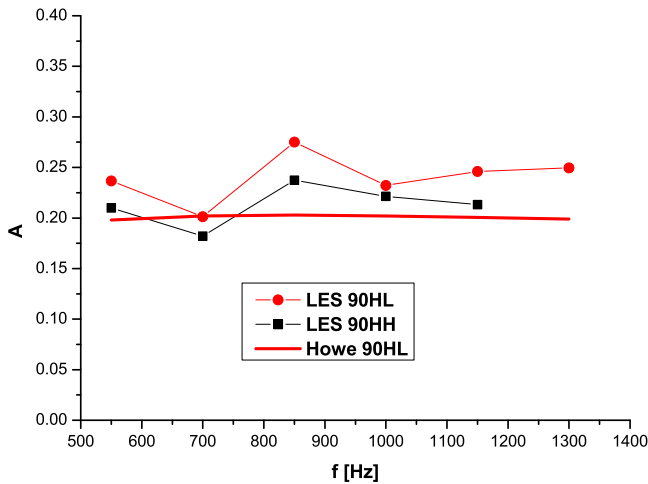


Figure 9. Effect of grazing flow (90°,  $Ma_b = 0.1$ ).

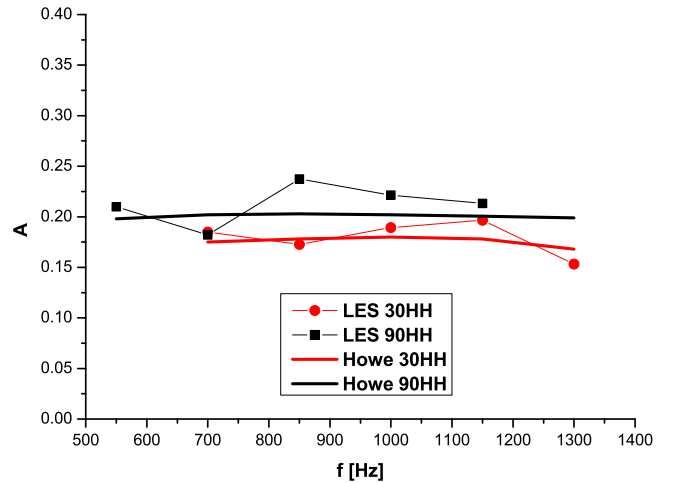


Figure 10. Effect of inclination angle ( $Ma_{cf} = 0.08$ ,  $Ma_b = 0.1$ ).

tions are almost coincident.  $30^\circ$  geometry anyhow is less influenced by frequency of excitation and the differences in absorption are limited with an average value of 0.05. These differences becomes larger at low bias flow especially at high frequencies. As noticed comparing Fig.11 and Fig.6 in fact, the increase in absorption reducing the bias flow is smaller at  $30^\circ$  where the effects of the inclined walls clearly reduce absorption properties also in the limit of no bias flow.

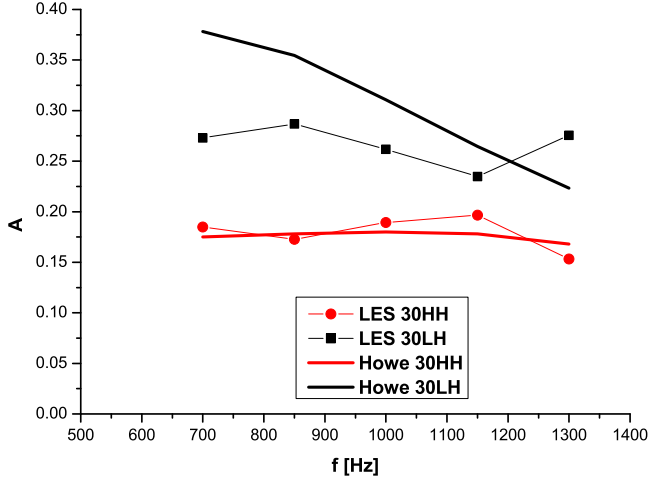


Figure 11. High and low bias flow absorption ( $30^\circ$ ,  $Ma_{cf} = 0.08$ ).

## PARALLEL WAVE

As already hinted in the introduction, main pressure waves travel along combustor axis. It is hence fundamental to assess the perforated liner acoustic behaviour also in case of parallel running excitation. In this case however exploiting a bi-periodic arrangement is not easy since the periodic boundaries should generate the acoustic forcing as well. That is why the single hole model previously described was abandoned for a more standard set-up exploiting lateral periodicity only and including a proper inlet and outlet boundary for the grazing flow as described in Fig.12.

In such a scheme the level of acoustic damping introduced by the plate is related to the number of hole rows included in the model, the higher the number of row the higher the absorption, so ideally it would be necessary to include the same amount of rows of the liner of interest. In this analysis, a parallel experimental campaign investigating the same perforation on a cylindrical liner with 18 rows [13] was chosen as a reference. However including all 18 rows would have been infeasible for computational cost reasons since maintaining the same amount of cells per hole as the normal wave set-up would have resulted in  $14 \cdot 10^6$  cells in the computational grid. It was hence decided to explore the behaviour of a 4 rows plate only. Also the investigated condi-

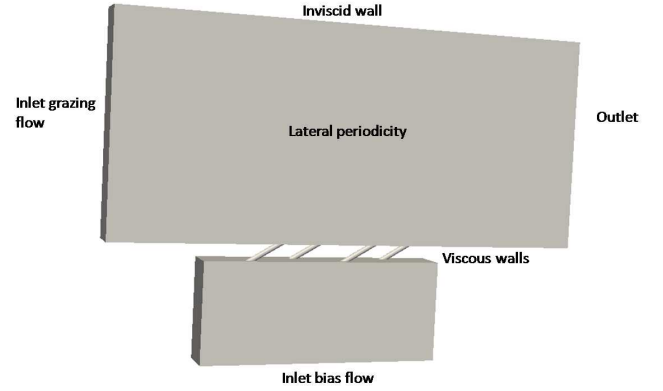


Figure 12. Parallel wave set-up.

tion was limited to the condition 30HH under acoustic forcing at 1000 Hz.

## Two source technique

With a parallel running wave, it is not possible to neglect the transmitted acoustic wave and the number of parameters to completely characterize acoustically the plate is increased ( $R^+$ ,  $R^-$ ,  $t^+$ ,  $t^-$  in Fig.13) thus a more complex post-processing technique needs to be applied. The two-source technique, already proposed and implemented to post-process experimental measurements by [36, 37], is hence employed.

This technique consists in exciting the plate twice, once imposing a forcing from the inflow (Fig.13(a)) and then moving the speakers at the outflow boundary (Fig.13(b)). The role of

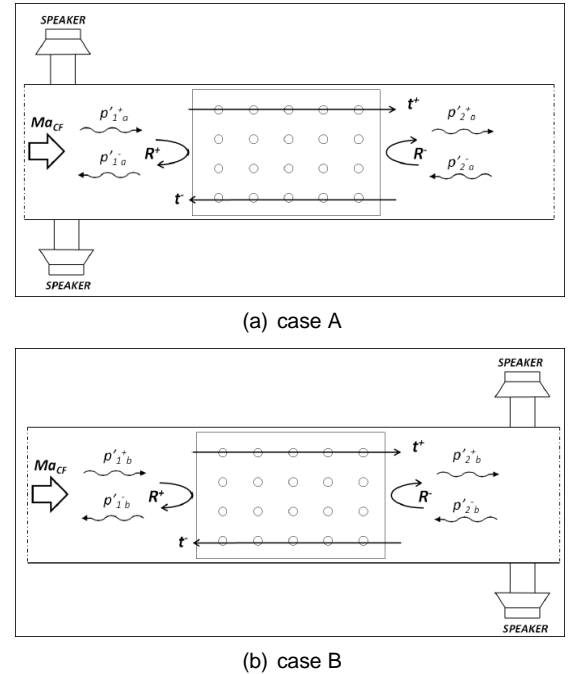


Figure 13. Schematic of the Two-source technique.

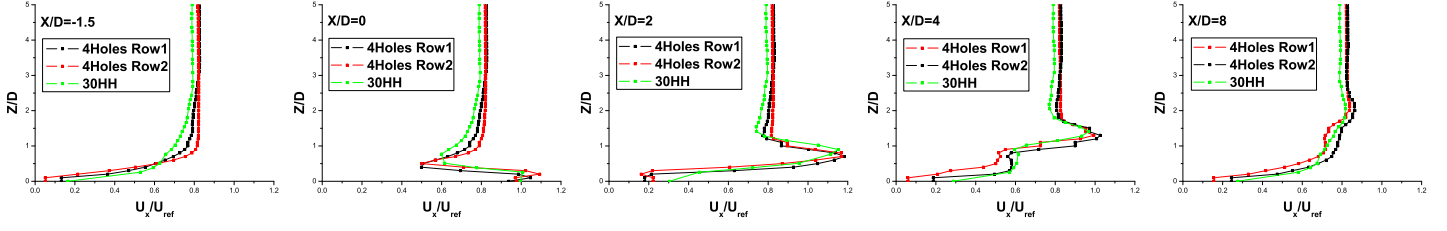


Figure 14. Mean streamwise velocity profiles for 90° case.

the speakers is played by the boundary conditions: in case A a fluctuating velocity inlet is providing the acoustic forcing while in case B perturbations are introduced by means of an oscillating pressure outlet. In such a way it is possible to compute the concordant and discordant running pressure waves exploiting the multi-microphone technique upstream and downstream of the liner separately. Eqs.9 can be used to compute the acoustic properties of the plate to finally calculate the energy dissipation coefficient from Eq.10.

$$\begin{aligned}
 R^+ &= \frac{p'_{1,a}p'_{2,b} - p'_{1,b}p'_{2,a}}{p'_{1,a}p'_{2,b} - p'_{1,b}p'_{2,a}} \\
 R^- &= \frac{p'_{2,b}p'_{1,a} - p'_{2,a}p'_{1,b}}{p'_{1,a}p'_{2,b} - p'_{1,b}p'_{2,a}} \\
 t^+ &= \frac{p'_{2,a}p'_{2,b} - p'_{2,b}p'_{2,a}}{p'_{1,a}p'_{2,b} - p'_{1,b}p'_{2,a}} \\
 t^- &= \frac{p'_{1,a}p'_{1,b} - p'_{1,b}p'_{1,a}}{p'_{1,a}p'_{2,b} - p'_{1,b}p'_{2,a}}
 \end{aligned} \quad (9)$$

$$\alpha^\pm = 1 - \left( \frac{1 \mp Ma}{1 \pm Ma} \|R^\pm\|^2 + \|t^\pm\|^2 \right) \quad (10)$$

### Flow field analysis

First analysis was conducted on the free simulation in order to verify that the mean cross flow was consistent with the chosen flow conditions.

Velocity profiles at various positions along the centerline of the first two rows of holes were extracted and compared in Fig.14 with the bi-periodic profiles already shown. Except for the  $x/D = -1.5$  where the multihole simulation shows a flatter profile due to non complete development of the boundary layer, the profiles for the single hole and the multihole case basically coincide, confirming that the artificially generated cross-flow is realistic.

### Acoustic results

The results obtained applying the two-source technique are reported in Tab.3. Very high transmission coefficient character-

ize both the progressive and regressive direction. It is interesting to note how the reflectivity of the plate is not symmetric and the upstream reflectivity is much higher than the downstream one. Combining those results it is possible to obtain the energy dissipation coefficient that shows to be more than double for the concordantly running acoustic wave. This difference between concordant and discordant dissipation coefficient is reported also in [14] for a 90° perforation at lower  $Ma_b$ . They showed a less stressed difference than in this case but the slanted angle certainly represent a source of additional non symmetric effects. Further analysis are required to reduce the obtained data in such a way to be compared with reference experiments conducted on a 18 rows plate [13].

	Modulus	Phase [rad]
$R^+$	<b>0.036</b>	<b>2.586</b>
$R^-$	<b>0.0197</b>	<b>0.415</b>
$t^+$	<b>0.985</b>	<b>0.004</b>
$t^-$	<b>0.969</b>	<b>-0.025</b>
$\alpha^+$	<b>0.0288</b>	
$\alpha^-$	<b>0.0605</b>	

Table 3. Acoustic properties of the multi-hole plate.

### CONCLUSIONS

An analysis about the acoustic behaviour of multi-perforated plates have been performed exploiting Large Eddy Simulation. The open-source OpenFOAM® platform was used to implement the necessary numerical techniques.

The study was started from a bi-periodic single hole domain under normal to the plate acoustic forcing. Sensitivity to the hole arrangement (in-line and staggered),  $Ma_b$  (0.05-0.1),  $Ma_{cf}$  (0-0.08) and hole inclination angle (90° and 30°) have been ex-

plored. In terms of acoustic absorption the hole arrangement and the cross-flow effects are small and can be neglected. On the contrary the most efficient way to enhance the absorption properties of the perforated plate is to decrease the bias flow: in fact moving from high to low bias the absorption coefficient is almost doubled reaching values above 0.35 for the 90° geometry. The reduction in perforation angle reduces the absorption as well but the effect is limited at least at the high bias condition which is more relevant for actual effusion cooling systems.

A plate with 4 holes at 30° under parallel running acoustic wave forcing was studied too, showing a pronounced asymmetric behaviour with the progressive energy absorption coefficient halving the regressive one.

## ACKNOWLEDGMENTS

The reported work was performed within the European research project *Knowledge for Ignition, Acoustic, and Instabilities - KIAI* (RTD-Project 7<sup>th</sup> FP, Contract No. 211843). The permission for the publication is gratefully acknowledged by the authors. The authors would like to thank PhD F. Simonetti for sharing the results obtained with the lumped acoustic approach.

## REFERENCES

- [1] Bellucci, V., Paschereit, C. O., and Flohr, P., 2004. "Numerical and experimental study of acoustic damping generated by perforated screens". *AIAA Journal*, **42**(8), pp. 1543–1549.
- [2] Howe, M. S., 1979. "On the theory of unsteady high Reynolds number flow through a circular aperture". *Proceedings of the Royal Society of London*, **366**, pp. 205–223.
- [3] Jing, X., and Sun, X., 2000. "Effect of plate thickness on impedance of perforated plates with bias flow". *AIAA Journal*, **38**(9), pp. 1573–1578.
- [4] Eldredge, J., and Dowling, A., 2003. "The absorption of axial acoustic waves by a perforated liner with bias flow". *Journal of Fluid Mechanics*, **485**, pp. 307–335.
- [5] Mendez, S., and Eldredge, J. D., 2009. "Acoustic modeling of perforated plates with bias flow for large-eddy simulations". *Journal of Computational Physics*, **228**, pp. 4757–4772.
- [6] Andreini, A., Bianchini, C., Facchini, B., and Simonetti, F., 2011. "Assessment of numerical tools for the evaluation of the acoustic impedance of multi-perforated plates". *ASME Turbo Expo 2011: Power for Land, Sea and Air*(GT2011-46303).
- [7] Gunasekaran, B., and McGuirk, J. J., 2011. "Mildly-compressible pressure-based cfd methodology for acoustic propagation and absorption prediction". *ASME Turbo Expo*(GT2011-45316).
- [8] Scarpato, A., Ducruix, S., and Schuller, T., 2011. "Ales based sound absorption analysis of high-amplitude waves through an orifice with bias flow". *ASME Turbo Expo*(GT2011-45639).
- [9] Mazdeh, A., and Kashani, R., 2011. "Distributed parameter acoustic modeling of a perforation with bias flow". *ASME Turbo Expo*(GT2011-46649).
- [10] Bhayaraju, U., Schmidt, J., Kashinath, K., and Hochgreb, S., 2010. "Effect of cooling liner on acoustic energy absorption and flame response". *ASME Turbo Expo*(GT2010-22616).
- [11] Heuwinkel, C., Enghardt, L., Bake, F., Sadig, S., and Gerendas, M., 2010. "Establishment of a high quality database for the modelling of perforated liners". *ASME Turbo Expo*(GT2010-22329).
- [12] Rupp, J., Carrotte, J., and Macquisten, M., 2011. "The use of perforated damping liners in aero gas turbine combustion systems". *ASME Turbo Expo*(GT2011-45488).
- [13] Andreini, A., Facchini, B., Ferrari, L., Lenzi, G., Simonetti, F., and Peschiulli, A., 2012. "Experimental investigation on multi-perforated liner geometries for aero-engines. Part I: Evaluation of global acoustic parameters". *ASME Turbo Expo 2012: Power for Land, Sea and Air*(GT2012-69853).
- [14] Heuwinkel, C., Enghardt, L., Rohle, I., Muhlbauer, B., Noll, B., Aigner, M., and Busse, S., 2008. "Comparison of experimental and numerical results concerning the damping of perforated liners with bias flow". *ASME Turbo Expo*(GT2008-50585).
- [15] Facchini, B., Tarchi, L., and Toni, L., 2009. "Investigation of circular and shaped effusion cooling arrays for combustor liner application - Part 1: Experimental analysis". *Proceedings of ASME Turbo Expo 2009: Power for Land, Sea and Air*(GT2009-60037).
- [16] Andreini, A., Bianchini, C., Ceccherini, A., Facchini, B., and Mangani, L., 2009. "Investigation of circular and shaped effusion cooling arrays for combustor liner application - Part 2: Numerical analysis". *Proceedings of ASME Turbo Expo 2009: Power for Land, Sea and Air*(GT2009-60038).
- [17] Eldredge, J. D., Bodony, D. J., and Shoeybi, M., 2007. "Numerical investigation of the acoustic behavior of a multi-perforated liner". *13th AIAA/CEAS Aeroacoustic Conference*(3683).
- [18] Luong, T., Howe, M., and McGowan, R., 2005. "On the Rayleigh conductivity of a bias-flow aperture". *Journal of Fluids and Structures*, **21**, pp. 769–778.
- [19] Weller, H. G., Tabor, G., Jasak, H., and Fureby, C., 1998. "A tensorial approach to computational continuum mechanics using object-oriented techniques". *Computers in Physics*, **12**(6).
- [20] Fureby, C., Weller, H. G., Tabor, G., and Gosman, A. D., 1997. "A comparative study of subgrid scale models in ho-

- ogeneous isotropic turbulence”. *Physics of Fluids*, **9**(5), pp. 1416–1429.
- [21] Fureby, C., 1996. “On subgrid scale modeling in large eddy simulations of compressible fluid flow”. *Physics of Fluids*, **8**(5), pp. 1300–1311.
- [22] Nicoud, F., and Ducros, F., 1999. “Subgrid-scale stress modelling based on the square of the velocity gradient tensor”. *Flow, Turbulence and Combustion*, **62**, pp. 183–200.
- [23] Sagaut, P., 2005. “Large eddy simulation for incompressible flows”. *Springer*.
- [24] Poinso, T. J., and Lele, S. K., 1992. “Boundary conditions for direct simulations of compressible viscous flows”. *Journal of Computational Physics*, **101**, pp. 104–129.
- [25] Yoo, C., Wang, Y., Trounev, A., and Im, H., 2005. “Characteristic boundary conditions for direct simulations of turbulent counterflow flames”. *Combustion Theory and Modeling*, **9**, pp. 617–646.
- [26] Thompson, K. W., 1987. “Time-dependent boundary conditions for hyperbolic systems”. *Journal of Computational Physics*, **68**, pp. 1–24.
- [27] Thompson, K. W., 1990. “Time-dependent boundary conditions for hyperbolic systems II”. *Journal of Computational Physics*, **89**, pp. 439–461.
- [28] Lodato, G., Domingo, P., and Vervisch, L., 2008. “Three dimensional boundary conditions for direct and Large-Eddy Simulation of compressible viscous flows”. *Journal of Computational Physics*, **227**, pp. 5015–5143.
- [29] Hughes, I., and Dowling, A., 1990. “The absorption of sound by perforated linings”. *Journal of Fluid Mechanics*, **218**, pp. 299–335.
- [30] Leppington, F., and Levine, H., 1973. “Reflexion and transmission at a plane screen with periodically arranged circular or elliptical apertures”. *Journal of Fluid Mechanics*, **61**, pp. 109–127.
- [31] Dassé, J., Mendez, S., and Nicoud, F., 2008. “Large-Eddy Simulation of the Acoustic Response of a Perforated Plate”. *Proceedings of the 14th AIAA/CEAS Aeroacoustic Conference*, AIAA Paper(2008-3007).
- [32] Liu, N., Hanjalic, K., Borello, D., and Tao, Z., 2009. “Large-eddy simulation of periodic discrete-hole effusion without and with rotation”. *8th European Turbomachinery Conference*.
- [33] Mendez, S., and Nicoud, S., 2008. “Adiabatic homogeneous model for the flow around a multi-perforated plate”. *AIAA Journal*, **46**(10), pp. 2623–2633.
- [34] Jang, S. H., and Ih, J. G., 1998. “On the multiple microphone method for measuring in-duct acoustic properties in the presence of mean flow”. *Journal of Acoustical Society of America*, **103**(3), pp. 1520–1526.
- [35] Mendez, S., and Nicoud, F., 2008. “Large-eddy simulation of a bi-periodic turbulent flow with effusion”. *Journal of Fluid Mechanics*, **598**, pp. 27–65.
- [36] Chung, J. Y., and Blaser, D. A., 1980. “Transfer function method of measuring in-duct acoustic properties. i. theory”. *Journal of the Acoustical Society of America*, **68**, p. 907:913.
- [37] Chung, J. Y., and Blaser, D. A., 1980. “Transfer function method of measuring in-duct acoustic properties. ii. experiments”. *Journal of the Acoustical Society of America*, **68**, p. 914:920.